Theoretical Study of Propellant Behavior during Thrust Chamber Depressurization

TSUYOSHI HIROKI* AND EDWARD A. FLETCHER†
University of Minnesota, Minneapolis, Minn.

A mathematical model that permits computation of burning rates of solid-propellant rocket motors during pressure transients is presented. The conservation equations in the solid and the gas phases are coupled with the chamber over-all mass balance equation. The method is used to compute the burning rate behavior during rapid depressurizations. The results of the computations are used to obtain *dP/dt*—extinguishment limits of solid propellants in terms of appropriate parameters. The agreement with the experimental quenching limit data is good.

Nomenclature

A = $K\Delta\bar{h}^0\bar{P}_1{}^n k_g/C_p{}^2\bar{T}_w{}^{(n+1)}R^n\bar{G}_1{}^2$
A_p = propellant surface area
A (with appropriate subscript) = area
$A_1, A_2, \ldots$ = defined by Eqs. (28) and following
C = specific heat capacity of the solid propellant
C_p = specific heat capacity of the gas
C_1 = $[2/(\gamma-1)]^{1/(\gamma-1)}[2\gamma/R(\gamma+1)]^{1/2}$
C_2 = $\bar{\rho}_s k_s \bar{P}_1{}^{2m}/C\bar{G}_1{}^2$
C_3 = $C_2(C_1V_c/A_p)^{2m/(m-1)}$
C_{12} = $[2\gamma R\bar{T}_f/(\gamma+1)]^{1/2}[2/(\gamma-1)]^{1/(\gamma-1)}$
D_g = $\bar{P}_1 k_g/t^*C_p{}^2\bar{T}_w\bar{G}_1{}^2$
D_s = $\bar{\rho}_s k_s/Ct^*\bar{G}_1{}^2$
$\mathfrak{D}$ = diffusion coefficient
E = dimensionless activation energy
f_s = heat flux to the solid in von Elbe's model
G = dimensionless mass flux
h = dimensionless specific enthalpy
Δh_w = dimensionless enthalpy change in the surface reaction
Δh^0 = dimensionless enthalpy change in the gas phase reaction
K = pre-exponential coefficient in reaction rate equation
k = thermal conductivity
m = pressure exponent of the burning rate in the Vieille equation
m (with appropriate subscript) = mass fraction
$\dot{m}$ (with appropriate subscript) = mass flow rate of exhausted gas
n = kinetic order of the chemical reaction
P = dimensionless pressure
q = internal energy of the solid in von Elbe's model
R = gas constant
r = $(P_2/P_1)^{(1-m)}$
t = dimensionless time $[t^* = r/C_{12}(1-r)]$
T = dimensionless temperature
V_c = thrust chamber volume
W_r = chemical reaction rate
x = dimensionless space coordinate
y = $(1/G)(dT/dx)$
γ = heat capacity ratio
θ = $(T-T_i)(T_w-T_i)$
λ = $G[\bar{G}_1{}^2\bar{T}_w R^n(\Delta\bar{h}^0)^{(n-1)}/\bar{P}_1{}^n K C_p{}^{(n-2)}k_g]^{1/2}/P^{n/2}$
λ_0 = $\lambda P^{n/2}/G$
ξ = $T_\infty - T$
ρ = density
τ = t/D_s
ϕ = dimensionless strength of heat source

Superscripts

* = nondimensionalizing quantity
$(\bar{\ })$ = real quantity
0 = standard reference state

Subscripts

f = adiabatic flame property
g = in the gas phase
i = ambient
pr = products
r = reactants
s = in the solid phase
t = throat
v = vent
w = at the surface
1 = initial steady operating state of the system
2 = steady operating condition corresponding to the expanded nozzle area
∞ = used with T means flame temperature during a transient

Received May 31, 1968; revision received March 3, 1969. This paper contains material taken from the Ph.D. thesis of T. Hiroki. We are grateful to P. L. Blackshear Jr. who suggested that we undertake numerical computations with the variable flame temperature model, and to M. L. Stein of the University's Numerical Analysis Center for his cooperation in making the facility available to us.

* Research Assistant; now with Ishikawajima-Harima Heavy Industries, Tokyo, Japan.

† Professor, Department of Mechanical Engineering. Associate Fellow AIAA.

Introduction

SOLID-PROPELLANT rocket motors can be quenched by a rapid decrease of the chamber pressure. Depressurization can be achieved by enlarging the throat. If depressurization is fast, the motor will quench even though the steady-state burning chamber pressure corresponding to the enlarged throat is above the low-pressure limit of stable combustion. Ciepluch[1,2] determined critical depressurization rates needed to quench typical ammonium perchlorate composite propellants. The critical depressurization rate was almost proportional to the initial chamber pressure; the critical time was nearly independent of the initial chamber pressure.

Information about burning rates during pressure transients should be helpful in understanding this phenomenon. Von Elbe[3] proposed a model to predict transient burning rates during moderately fast pressure changes. He assumed that the temperature profiles in the solid were the same as those of the steady state at the corresponding burning rate and that the heat flux from the gas phase is the same as that in the steady state at the corresponding burning rate. He derived

an equation for the transient burning rate in an explicit form. His burning rate is determined by the instantaneous chamber pressure and its time derivative; burning rates during depressurizations are lower than the steady-state burning rates at the corresponding pressures. The quench limit was assumed to be the point at which the burning rate becomes zero. The essential feature of von Elbe's model can be understood with reference to the integral form of the energy equation in the solid,

$$C\bar{G}(\bar{T}_w - \bar{T}_i) = f_s - dq/d\bar{t}$$

where f_s is the heat flux to the grain just inside the propellant surface, and q is the internal energy in the solid. Since $dq/d\bar{t}$ is positive during depressurization, if f_s has its steady-state value at the corresponding burning rate, the burning rate $\bar{G}$ during depressurization must be smaller than the steady-state rate.

Since $dq/d\bar{t}$ was evaluated from the steady-state temperature profiles, it had a nonzero value at $\bar{t} = 0$ (the time when depressurization started). Thus, this model predicts a discontinuous change in the burning rate at $\bar{t} = 0$ if $d\bar{P}/d\bar{t}$ undergoes a discontinuous change. However, $dq/d\bar{t}$ evaluated from the solution of the nonsteady heat conduction equation is zero and, hence, the burning rate does not change discontinuously; applicability of this quasi-steady model to a rapid depressurization process, especially up to a quench point, is questionable.

A small perturbation method[4] has also been used in modeling nonsteady combustion in connection with combustion instability to compute[5] the first-order response of the burning rate to depressurization.

Solid-propellant rocket motors can also be quenched by reduction of the chamber pressure to below some critical pressure in the phenomenon called L^* extinguishment.[6] The depressurization rate is immaterial. Coates, Polzien, and Price[7] have discussed combustion termination by nozzle area variation. Both kinds of quenches were considered. They implicitly assumed that the critical depressurization time observed with one motor is valid for another. This is probably not true. Consider two extreme cases. If $\bar{P}_2/\bar{P}_1$ is nearly one, even extremely large depressurization rates may not produce a quench. If it could be achieved at all, it could be done only with a very small chamber free volume. On the other hand, if $\bar{P}_2/\bar{P}_1$ is nearly zero, a very small depressurization rate may produce a quench. Thus, the limit depends, not only on the depressurization rate, but on the motor configuration as well. This paper presents a method of computing burning rates during rapid depressurization. The effects of motor geometry are included by coupling the conservation equations in the gas and solid phases with the chamber mass conservation equation. The results of the burning rate computations are used to determine quench limits, which are correlated here in a way that has greater generality than critical time data. Additional details, including computer programs are described elsewhere.[8]

Mathematical Model

A one-dimensional model is used. A one-dimensional model is probably valid for most configurations because the flame is thin compared with typical motor dimensions. Thermodynamic and transport properties are assumed constant. A single-step reaction of the order n (which may have fractional values) is assumed. Molecular weights of gaseous reactant and product are assumed equal. The propellant surface temperature is assumed to stay constant. No solid phase reaction is considered. The burning rate is determined as a connecting coefficient of the conservation equations in the solid and gas phases which satisfies the boundary conditions imposed at the propellant surface.

In the gas phase the continuity equation is

$$\partial\bar{\rho}/\partial\bar{t} + \partial\bar{G}/\partial\bar{x} = 0 \tag{1}$$

Continuity for the reactant is given by

$$\bar{\rho}\,\partial m_r/\partial\bar{t} + \bar{G}\,\partial m_r/\partial\bar{x} - \bar{\rho}\mathfrak{D}\,\partial^2 m_r/\partial\bar{x}^2 = \bar{W}_r(\bar{\rho}_r,\bar{T}) \tag{2}$$

where

$$W_r = -K\bar{\rho}_r{}^n \exp(-\bar{E}/\bar{T})$$

is the rate of formation of the reactant.

The diffusion-thermo effect and kinetic energy of the gas are assumed negligible. If heat capacities of reactant and product are the same, the energy equation is

$$\bar{\rho}C_p\frac{\partial\bar{T}}{\partial\bar{t}} + \bar{G}C_p\frac{\partial\bar{T}}{\partial\bar{x}} - \frac{\partial\bar{P}}{\partial\bar{t}} - k_g\frac{\partial^2\bar{T}}{\partial\bar{x}^2} = -\Delta\bar{h}^0\,W_r \tag{3}$$

The flame is thin compared with the expansion wave caused by enlargement of the exhaust nozzle. The chamber pressure is, therefore, assumed to be uniform; the momentum equation can be removed.

The boundary conditions at the propellant surface are derived from

Continuity of mass flux:

$$\bar{G}_s(\bar{t}) = \bar{G}_g(0,\bar{t}) \tag{4}$$

Continuity of temperature:

$$\bar{T}_s(0,\bar{t}) = \bar{T}_g(0,\bar{t}) = \bar{T}_w \tag{5}$$

Continuity of species mass flux:

$$\bar{G}_s(\bar{t}) = m_r\bar{G}_g(0,\bar{t}) - \bar{\rho}\mathfrak{D}(\partial m_r/\partial\bar{x})_w \tag{6}$$

Energy balance:

$$k_s(\partial\bar{T}/\partial\bar{x})_{s,w} = k_g(\partial\bar{T}/\partial\bar{x})_{g,w} - \Delta\bar{h}_w\bar{G}_s(\bar{t}) \tag{7}$$

Let the enthalpy of the gas be

$$\bar{h} = C_p\bar{T} + m_r\Delta\bar{h}^0$$

Combination of Eqs. (2) and (3) yields, if the Lewis number is assumed to be one,

$$\bar{\rho}\,\partial\bar{h}/\partial\bar{t} - \partial\bar{P}/\partial\bar{t} + G\,\partial\bar{h}/\partial\bar{x} - (k_g/C_p)\,\partial^2\bar{h}/\partial\bar{x}^2 = 0 \tag{8}$$

with the boundary condition at the propellant surface,

$$(\bar{h}_r{}^0 + C_p\bar{T}_w - \Delta\bar{h}_w)\bar{G}_s - k_s\left(\frac{\partial\bar{T}}{\partial\bar{x}}\right)_{s,w} = \bar{G}_s\bar{h}_w - \frac{k_g}{C_p}\left(\frac{\partial\bar{h}}{\partial\bar{x}}\right)_{g,w} \tag{9}$$

In the solid, with the space coordinate fixed with respect to the solid, the energy equation is

$$\bar{\rho}_s C\,\partial\bar{T}/\partial\bar{t} = k_s\,\partial^2\bar{T}/\partial\bar{x}^2 \tag{10}$$

with the boundary condition,

$$\bar{T} = \bar{T}_w \quad \text{at} \quad \bar{x} = -\int_0^{\bar{t}}\frac{\bar{G}_s}{\bar{\rho}_s}\,d\bar{t} \tag{11}$$

Since the chamber pressure is not a prescribed function of time, these equations must be coupled with the chamber conservation equations. If depressurization is achieved by a sudden enlargement of the exhaust nozzle area, the depressurization rate depends on the enlarged nozzle area. It has been shown that the pressure vs temperature relation in the chamber during depressurization has minor effects on the burning rate vs chamber pressure relationship.[9] It is therefore assumed for simpliciy that the over-all chamber temperature stays constant. The ambient pressure is assumed to be zero. Then the mass conservation equation for the whole chamber is given by[8,9]

$$\frac{1}{\bar{P}_1C_{12}}\left(\frac{\bar{P}_2}{\bar{P}_1}\right)^{(1-m)}\frac{d\bar{P}}{d\bar{t}} = \left(\frac{\bar{P}_2}{\bar{P}_1}\right)^{(1-m)}\frac{\bar{G}}{\bar{G}_1} - \frac{\bar{P}}{\bar{P}_1} \tag{12}$$

where C_{12} is a constant that depends on propellant properties and motor geometry.

In the derivation of Eq. (12), the steady-state burning rates were assumed to follow the Vieille equation. It turns out that the present model, if applied to the steady state, produces the same steady-state burning rate equation.

To nondimensionalize the equation, the following nondimensionalizing quantities are selected:

$$P^* = \bar{P}_1;\ T^* = \bar{T}_w;\ G^* = \bar{G}_1;\ E^* = \bar{T}_w;\ h^* = C_p\bar{T}_w$$

$$x_s{}^* = k_s/C\bar{G}_1;\ x_g{}^* = k_g/C_p\bar{G}_1$$

Different lengths were used in the solid and gas phase because the characteristic thermal layer thicknesses are different in the two phases. t^* is chosen such that $dP/dt = -1$ at $t = 0$. Then t^* is the characteristic time for the depressurizations. It is given by $t^* = r/C_{12}(1 - r)$. The resulting nondimensional form of governing equation follows. In the gas phase,

$$[D_g\gamma/(\gamma - 1)](\partial/\partial t)(P/T) + \partial G/\partial x = 0 \tag{13}$$

$$D_g\left(\frac{\gamma}{\gamma - 1}\frac{P}{T}\frac{\partial T}{\partial t} - \frac{\partial P}{\partial t}\right) + G\frac{\partial T}{\partial x} - \frac{\partial^2 T}{\partial x^2} = A\left(\frac{P}{T}\right)^n m_r{}^n e^{-E/T} \tag{14}$$

and

$$D_g\left(\frac{\gamma}{\gamma - 1}\frac{P}{T}\frac{\partial h}{\partial t} - \frac{\partial P}{\partial t}\right) + G\frac{\partial h}{\partial x} - \frac{\partial^2 h}{\partial x^2} = 0 \tag{15}$$

where

$$D_g = \bar{P}_1 k_g/t^* C_p{}^2\bar{T}_w\bar{G}_1{}^2$$

and

$$A = K\Delta\bar{h}^0\bar{P}_1{}^n k_g/C_p{}^2\bar{T}_w{}^{(n+1)}R^n\bar{G}_1{}^2$$

The boundary conditions at the propellant surface become

$$G_s(t) = G_g(0,t) \tag{16}$$

$$T_s(0,t) = T_g(0,t) \tag{17}$$

$$(C/C_p)(\partial T/\partial x)_{s,w} = (\partial T/\partial x)_{g,w} - \Delta h_w G_s(t) \tag{18}$$

and

$$(\Delta h^0 - \Delta h_w + 1)G_s - \frac{C}{C_p}\left(\frac{\partial T}{\partial x}\right)_{s,w} + \left(\frac{\partial h}{\partial x}\right)_{g,w} = G_s h_{g,w} \tag{19}$$

In the solid,

$$D_s\,\partial T/\partial t = \partial^2 T/\partial x^2 \tag{20}$$

where

$$D_s = \bar{\rho}_s k_s/Ct^*\bar{G}_1{}^2$$

with the boundary condition

$$T = 1 \quad \text{at} \quad x = -\int_0^t \frac{G}{D_s}\,dt \tag{21}$$

Let $r = (P_2/P_1)^{(1-m)}$. Equation (12) becomes

$$(1 - r)dP/dt = rG - P \tag{22}$$

All time-dependent terms are associated with D_s and D_g. These parameters determine the magnitude of the departure of nonsteady burning rates from steady-state values. D_s and D_g represent the ratios of the temperature response times in the solid and gas phases to the characteristic time for depressurization. If one assumes as representative values $C = 0.3$ cal/g°C; $C_p = 0.5$ cal/g°C; $k_s = 9.8 \times 10^{-4}$ cal/°C sec cm; $k_g = 2.0 \times 10^{-4}$ cal/°C sec cm; $\bar{T}_w = 900$°K; and $\bar{\rho}_s = 1.7$ g/cm³;

$$D_s = 5.54 \times 10^{-3}/\bar{G}_1{}^2 t^*$$

$$D_g = 1.465 \times 10^{-9}\bar{P}_1/\bar{G}_1{}^2 t^*$$

where $\bar{G}_1$ is in g/sec cm², t^* is in sec, and $\bar{P}_1$ is in psia.

Typical ammonium perchlorate propellants quench when $d\bar{P}/d\bar{t}$ is about 7×10^4 psi/sec at $\bar{P}_1 = 500$ psia. At the quenching limit, then, $D_s = 0.827$ and $D_g = 1.0 \times 10^{-4}$.

The nondimensionalizing quantities were chosen so that all the derivatives and reaction terms are of the order one in the nondimensional equations. One may conclude the following: when $\bar{P}_1 \simeq 500$ psia, $\bar{G}_1 \simeq 1$ g/cm² sec, and if $d\bar{P}/d\bar{t} < 10^3$ psia/sec, the whole process is quasi-steady and the burning rate follows the steady-state law. If 10^4 psia/sec $< d\bar{P}/d\bar{t} < 10^7$ psi/sec, relaxation time in the gas is still negligible, but it cannot be neglected in the solid. If $d\bar{P}/d\bar{t} > 10^8$ psi/sec, relaxation times are not negligible in either phase. Since the quench occurs at $d\bar{P}/d\bar{t} \approx 10^5$ psi/sec, the terms associated with D_g can be neglected in this study. Then the gas phase equations (14) and (15) are reduced to

$$G\,dT/dx - d^2T/dx^2 - A\,(P/T)^n m_r{}^n e^{-E/T} = 0 \tag{23}$$

and

$$G\,dh/dx - d^2h/dx^2 = 0 \tag{24}$$

Since Eqs. (23) and (24) are ordinary differential equations, the boundary condition at $x = \infty$ must be evaluated.

Solution

The solution of Eq. (24) that assumes finite values at $x = \infty$ is $h = C_2$. The constant C_2 can be evaluated at $x = \infty$. Since $m_r = 0$ at $x = \infty$

$$h = T + \Delta h^0 m_r = T_\infty(t) \tag{25}$$

Combination of Eqs. (25) and (19) gives

$$\Delta h^0 - \Delta h_w - (T_\infty - 1) = (C/C_p)(1/G)(\partial T/\partial x)_{s,w} \tag{26}$$

The variation of T_∞ with time is given by Eq. (26). In the quasi-steady case, the right-hand side of Eq. (26) stays constant. Hence, T_∞ does not change. In the nonsteady state, the right-hand side increases with time; hence T_∞ decreases.

The preceding argument is based on the assumption that the time-dependent term in the gas phase is completely negligible in the entire space. However, the time-dependent term is the same order of magnitude as the other terms far from the propellant surface; the time-dependent terms predominate and the solution of the Eq. (14) at $x = \infty$ is

$$P^{(\gamma-1)}/T^\gamma = \text{const}$$

This is the isentropic relationship. This occurs very far from the surface, possibly outside the motor. The temperature of the gas at a distance where the time-dependent term is the same order of magnitude as the rest of the terms does not decrease as much as described by Eq. (26). The time-dependent terms also become nonnegligible near the end of the depressurization process. Hence, Eq. (26) gives the lower limit of T_∞. As an upper limit, constant flame temperature ($T_\infty = T_f$) will also be considered. Actual processes will be between these two limits. Except near the end of the depressurization process the lower limit is probably closest to reality.

We define the new variables

$$y = (1/G)dT/dx \text{ and } \xi = T_\infty - T$$

Then, elimination of m_r from Eqs. (23) and (25) gives

$$\frac{dy}{d\xi} = -1 + \frac{\exp[-E/(T_\infty - \xi)]}{\lambda^2(T_\infty - \xi)^n}\frac{\xi^n}{y} \tag{27}$$

During the depressurization λ may decrease. For small values of λ, the solutions of Eq. (27) are given by asymptotic series of the form[8]

$$y(\xi) = \frac{1}{\lambda}\,[A_0(\xi) + A_1(\xi)\lambda + A_2(\xi)\lambda^2 + \ldots] \quad (28)$$

The values at the propellant surface are obtained if A_0, A_1, etc. are evaluated at $\xi_w = (T_\infty - 1)$. They are given by

$$A_0(\xi_w) = \left[2\int_0^{\xi_w} \frac{\xi^n}{(T_\infty - \xi)^n} \exp[-E/T_\infty - \xi)]d\xi\right]^{1/2}$$

$$A_1(\xi_w) = -\int_0^{\xi_w} [A_0(\xi)/A_0(\xi_w)]d\xi$$

$$A_2(\xi_w) = \left[-\int_0^{\xi_w} A_1(\xi)d\xi - \frac{1}{2}A_1^2(\xi_w)\right]\Big/A_0(\xi_w)$$

$$A_3(\xi_w) = \left[-A_1(\xi_w)A_2(\xi_w) - \int_0^{\xi_w} A_2(\xi)d\xi\right]\Big/A_0(\xi_w)$$

$$A_4(\xi_w) = \left[-\int_0^{\xi_w} A_3(\xi)d\xi - \frac{1}{2}A_2(\xi_w) - A_1(\xi_w)A_3(\xi_w)\right]\Big/A_0(\xi_w)$$

etc. Comparison with the solution obtained by a finite-difference method indicated that asymptotic series (28) yields the best approximation when the first five terms are retained. It should be noted that A_0, A_1, etc. are functions of T_∞.

Combination of Eqs. (28) and (18) gives

$$\frac{C}{C_p}\frac{\lambda}{P^{n/2}}\left(\frac{\partial T}{\partial x}\right)_{s,w} = F(\lambda,T_\infty) \quad (29)$$

where

$$F(\lambda,T_\infty) = A_0(T_\infty) + [A_1(T_\infty) - \Delta h_w]\lambda + A_2(T_\infty)\lambda^2 + \ldots$$

If the temperature gradient in the solid at the propellant surface is evaluated, Eq. (29) can be solved for λ and the burning rate is given by

$$G = (\lambda/\lambda_0)P^{n/2} \quad (30)$$

The solution of the solid phase equation (20) with the moving boundary condition (21) is given by the use of a moving point heat source.

For convenience, the direction of the x coordinate is reversed so that the positive direction is toward the solid phase. The whole x space ($-\infty < x < \infty$) is used.

If new time τ and temperature (θ) scales are used, Eq. (20) becomes

$$\partial\theta/\partial\tau = \partial^2\theta/\partial x^2 \quad (31)$$

The initial values of θ are given by the solution of the steady-state equation. Hence,

$$\theta = \begin{cases} e^{-x} \text{ at } x \geq 0 \\ 1 \text{ at } x \leq 0 \end{cases} \quad (32)$$

The initial values for $x < 0$ were chosen so that the temperature was uniform outside the solid. To satisfy the boundary condition (21), a moving heat source with the strength ϕ is distributed along the trajectory of the propellant surface position (curve S of Fig. 1) on the $x - t$ plane.[8] Then the solution of Eq. (31) is given by the use of Green's function. The result is

$$\theta(x,\tau) = \theta_a(x,\tau) + \int_0^\tau K_1(x,x'_w,\tau,\tau'_w)\phi(\tau'_w)d\tau'_w \quad (33)$$

where

$$K_1(x,x',\tau,\tau') = e^{-(x-x')^2/4(\tau-\tau')}/2[\pi(\tau - \tau')]^{1/2}$$

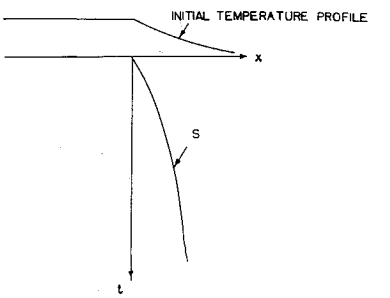

Fig. 1 Moving heat source coordinates.

and

$$\theta_a(x,\tau) = \int_{-\infty}^{\infty} \theta(x',0)K_1(x,x',\tau,0)dx'$$

Points (x'_w,τ'_w) are on curve S. The first integration θ_a is given explicitly by

$$\theta_a(x,\tau) = \frac{1}{2} + \frac{1}{2}e^{(\tau-x)} - \frac{1}{2}\,\mathrm{erf}\,\frac{x}{2\tau^{1/2}} + e^{(\tau-x)}\,\mathrm{erf}\,\frac{2\tau - x}{2\tau^{1/2}} \quad (34)$$

Along curve S, $\theta = 1$; hence Eq. (33) becomes

$$1 - \theta_a(x_w,\tau_w) = \int_0^{\tau w} K_1(x_w,x'_w,\tau_w,\tau'_w)\phi(\tau'_w d)\tau_w \quad (35)$$

Points (x_w,τ_w) and (x'_w,τ'_w) are given by

$$dx_w/d\tau_w = G(\tau_w);\; dx'_w/d\tau'_w = G(\tau'_w) \quad (36)$$

Equation (35) is the integral equation for ϕ if G is a known function of time. Initial condition (32) and boundary condition (21) gives

$$\phi = [1/(1 - \tau_r)](dT/dx)_{s,w} \quad (37)$$

Combination of Eqs. (37) and (29) yields

$$(1 - T_r)(C/C_p)(\lambda_0/P^{n/2})\phi = F(\lambda,T_\infty) \quad (38)$$

The burning rate is determined such that Eqs. (35, 36, and 38) are simultaneously satisfied. This can be done by following the numerical procedure outlined below.

Numerical Procedure

Suppose the computation has been completed up to $\tau = \tau_m$. Then τ_{m+1}, P_{m+1}, ϕ_{m+1}, $X_{w,m+1}$, $T_{\infty,m}$, and G_{m+1} are determined in the following way. Integration of Eq. (33) is split into two parts, from $\tau = 0$ to $\tau = \tau_m$ and from $\tau = \tau_m$ to $\tau = \tau_{m+1}$. The latter integral is approximated by

$$\frac{\phi_m + \phi_{m+1}}{2}\int_{\tau_m}^{\tau_{m+1}} K_1(x_w,x'_w,\tau_w,\tau'_w)d\tau'_w \quad (39)$$

Assuming constant G from τ_m to τ_{m+1},

$$x_{w,m+1} = x_{w,m} + G_m\Delta\tau \quad (40)$$

The integral becomes

$$(1/G_m)\,\mathrm{erf}[G_m(\Delta\tau)^{1/2}/2]$$

Then Eq. (35) becomes

$$\frac{\phi_m + \phi_{m+1}}{2}\frac{1}{G_m}\,\mathrm{erf}[G_m(\Delta\tau)^{1/2}/2] = 1 - \theta_a(x_{w,m+1},\tau_{w,m+1}) - \int_0^{\tau m} K_1(x_{w,m+1},x'_w,\tau_{w,m+1},\tau'_w)d\tau' \quad (41)$$

The integral on the right-hand side can be evaluated numerically. Then ϕ_{m+1} can be obtained from Eq. (35). P_{m+1} is

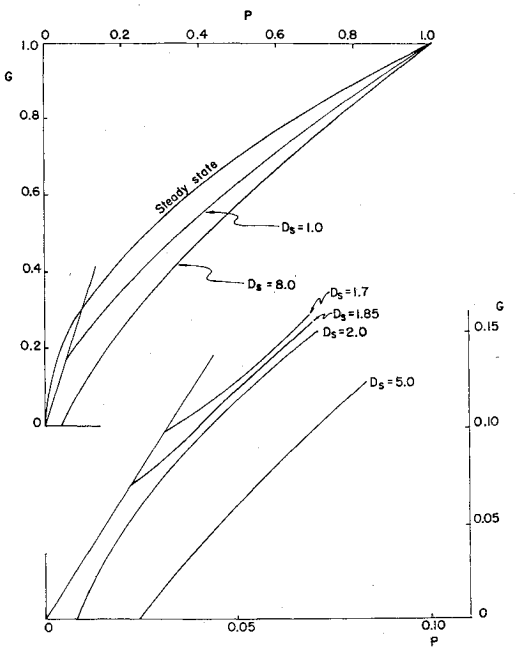

Fig. 2 Variation of burning rate with pressure during depressurization at various depressurization rates. The upper part of the figure shows the gross effect. The lower part is a detailed view of the lower left-hand corner. The straight line originating at the origins is the mass flux through the expanded nozzle. n = 1.0, E = 5.56, Δh_w = 0, P_2/P_1 = 0.1, E = 5000°K, T_i = 300°K, T_* = 900°K, T_f = 2700°K, C = 0.3 cal/g°K, C_p = 0.5 cal/g°C.

given by

$$P_{m+1} = P_m + [D_s/(1 - r)](rG - P)\Delta\tau$$

λ_{m+1} is obtained by solving

$$(C/C_p)(1 - T_i)\phi_{m+1}\,\lambda_0/P_{m+1}^{n/2} = F(\lambda_{m+1}, T_{\infty m}) \qquad (42)$$

For the constant flame temperature model $T_{\infty,m+1} = T_f$.

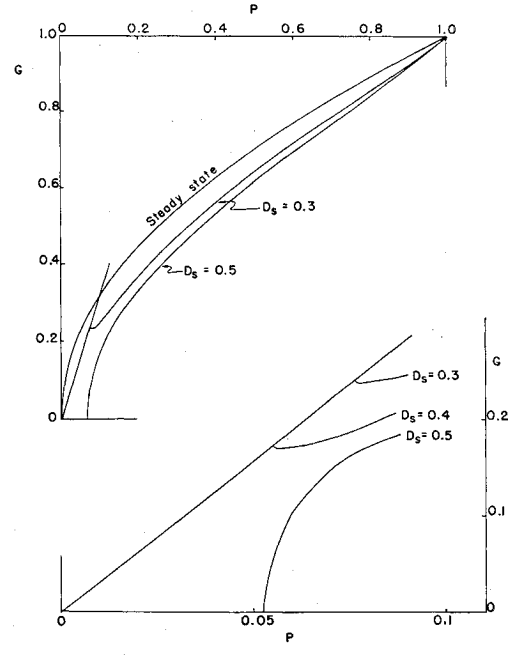

Fig. 3 Variation of burning rate with pressure during depressurization at various depressurization rates (variable temperature model). Same initial conditions as in Fig. 2.

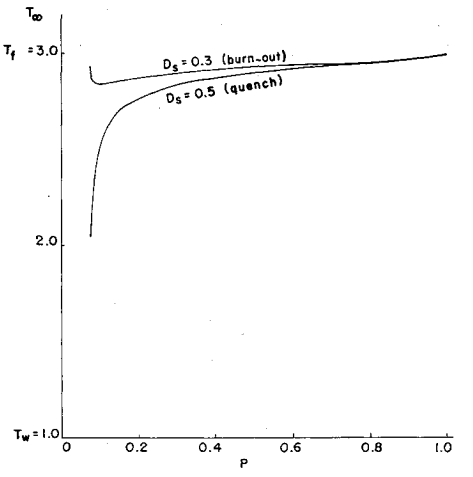

Fig. 4 Variation of flame temperature with chamber pressure during depressurization (variable temperature model). Initial conditions same as in Fig. 2.

For the varying flame temperature model, from Eq. (26)

$$T_{\infty,m+1} = T_f - (C/C_p)(1 - Ti)[(\phi_{m+1}/G_{m+1}) - 1] \qquad (43)$$

The burning rate is given by

$$G_{m+1} = (\lambda_{m+1}/\lambda_0)P_{m+1}^{n/2} \qquad (44)$$

In the actual computation, a predictor-corrector method was used to improve the accuracy.

Results

The input variables for the burning rate computations are $\bar{T}_i$, $\bar{T}_w$, $\bar{T}_f$, $\bar{E}$, $\Delta\bar{h}_w$, C/C_p, P_2/P_1, and D_s. Each took about three minutes on the Control Data 6600 computer. Computed burning rate vs chamber pressure curves are shown in Figs. 2 and 3 for typical cases. Figure 2 is for the constant flame temperature and Fig. 3 is for the variable flame temperature model. The upper figures show the over-all picture of the burning rate behaviors. The lower figures show the detailed behavior near the origin. If the burning rate becomes equal to the mass flow rate through the expanded nozzle, the chamber pressure will climb up to P_2 and a burn-out results. The computations were terminated when $|dP/dt| \leq 0.002$ in burn-out, or $G < 0.01$ in a quench. In

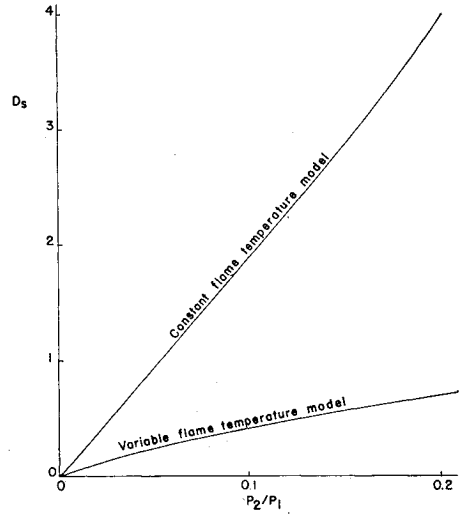

Fig. 5 Quench limits obtained with constant and variable flame temperature models. Initial conditions same as in Fig. 2.

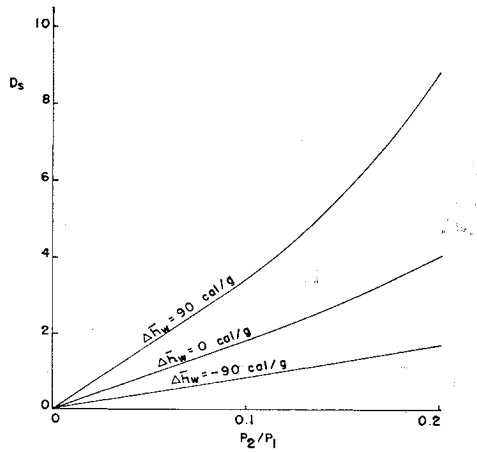

Fig. 6 Effect of heat of vaporization on the quench limit (constant flame temperature model). Same initial conditions as in Fig. 2.

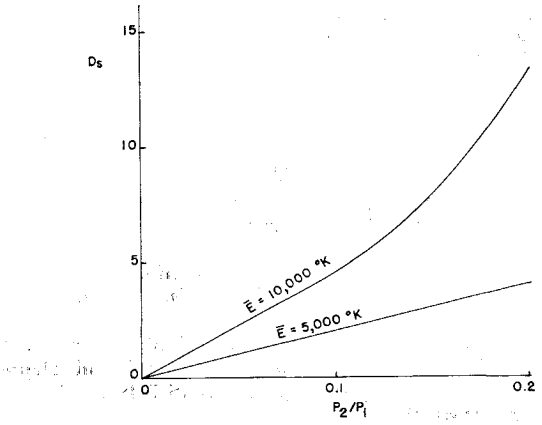

Fig. 7 Effect of variation of activation energy of gas phase reaction on quench limit (constant flame temperature model). Same initial conditions as in Fig. 2.

Fig. 4, the flame temperature is plotted against chamber pressures for typical cases. The flame temperature decreases considerably during depressurization, especially in a quench. In all cases, burning rates during depressurization are smaller than the steady-state values at the corresponding chamber pressures. The decreases in the burning rates are more drastic in the variable flame temperature model. A quench occurs when the value of D_s exceeds some critical value. The results of the burning rate computations were used to construct the quenching limit curve on the $D_s - P_2/P_1$ plane. The result is shown in Fig. 5 for a typical case. It is seen that the values of D_s at quench points for the variable temperature model are about one-fourth of the values for the constant flame temperature model. The quenching limit curves for different propellant properties were computed for the constant flame temperature model and are shown in Figs. 6–8. The critical depressurization parameter decreases as Δh_w decreases. In other words, a propellant is easier to quench when the surface reaction is exothermic, all other factors being the same. It also becomes easier to quench as the activation energy of the gas phase reaction decreases and as the reaction order increases.

Discussion

The present one-dimensional theory predicts that burning rates during depressurization should be smaller than the steady-state burning rates at the corresponding chamber pressures. Such behavior has been observed experimentally.[2]

The computed critical depressurization parameters D_s for a typical experiment ($P_2/P_1 = 0.1$) can be taken from Fig. 5, for example. The values of D_s are 1.85 for the constant flame temperature model and 0.45 for the variable flame temperature model. For typical propellants, these values correspond approximately to depressurization rates of 160,000 and 33,000 psi/sec Ciepluch[2] observed a critical depressurization rate of 70,000 psi/sec for a typical ammonium perchlorate propellant burning at a chamber pressure of 500 psia. Hence, both models give answers that are the right order of magnitude. It has also been observed that the critical time for a quench is independent of the initial pressure when the experiments are conducted with a motor that has a fixed free volume and propellant surface area. In this experiment, the depressurization rate, and P_2/P_1 are related. Using the definition of D_s, this relation is given by

$$D_s = C_3/\{(1/r - 1)^{2m/(1-m)} t^{*(1+m)/(1+m)}\} \qquad (45)$$

C_3 is a constant determined by the propellant properties and the motor geometry. If t^* is assumed to be constant, Eq. (45) gives the quenching limit curve on the $D_s \sim P_2/P_1$ plane, which is consistent with these experiments. The trend of this curve agrees with the quenching limit curves of Ref. 1. The present theory goes one step further, however. If the quenching limit curves on the $D_s \sim P_2/P_1$ plane are obtained for the same propellant but with different motors, they will fall on the same curve so long as depressurization rates are controlled in the same way.

In this study, the propellant surface temperature is assumed constant. If a functional relationship between the surface temperature and the burning rate is available, the present theory can accommodate this with slight modifications.

Conclusion

The present model suggests that burning rates of solid propellants during depressurization are lower than steady-state values because of the slow temperature readjustment in the solid. The flame temperature decreases considerably during depressurizations. Both the constant flame temperature model and the variable flame temperature model give the depressurization rates needed to quench propellants that are consistent with the experiments.

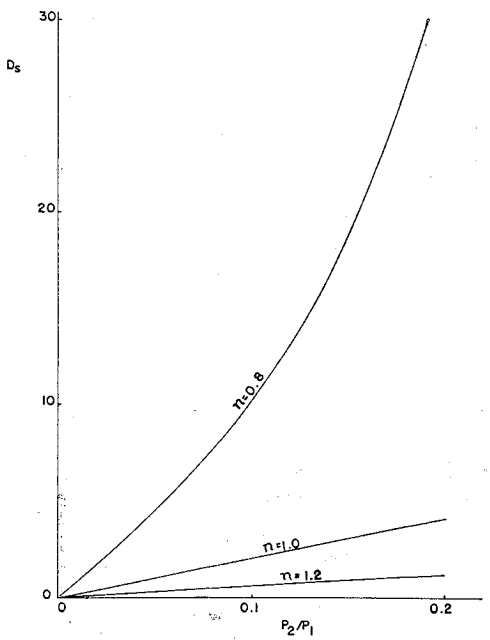

Fig. 8 Effect of gas phase reaction order (and pressure dependence of burning rate) on quench limit (constant flame temperature model).

References

[1] Ciepluch, C., "Effects of Rapid Pressure Decay on Solid Propellant Combustion," *ARS Journal*, Vol. 31, No. 11, Nov. 1961, pp. 1584–1586.

[2] Ciepluch, C., "Effect of Composition of Solid Propellants During a Rapid Pressure Decrease," TN D-1559, Dec. 1962, NASA.

[3] von Elbe, G., "Theory of Solid Propellant Ignition and Response to Pressure Transients," *Bulletin of the 19th ICRPG Solid Propulsion Conference*, CPIA Publication 18, July 1963, Vol. III, p. 95.

[4] Denison, M. R. and Baum, E., "A Simplified Model of Unstable Burning in Solid Propellants," *ARS Journal*, Vol. 31, No. 8, 1961, p. 1112.

[5] Capener, E. L., Dickinson, L. A., and Marxman, G. A., 'Propellant Combustion Phenomenon During Rapid Depressurization," Quarterly Report, Contract NAS 7-389, 1967, Stanford Research Institute.

[6] Anderson, F. A., Strehlow, R. A., and Strand, L. D., "Low Pressure Extinction," *AIAA Journal*, Vol. 1, No. 11, Nov. 1963, pp. 2669–2671.

[7] Coates, R. L., Polzien, R. E., and Price, C. F., "Design Procedure for Combustion Termination by Nozzle Area Variation," *Journal of Spacecraft and Rockets*, Vol. 3, No. 3, March 1966, pp. 419–425.

[8] Fletcher, E. A. and Hiroki, T., "A Theoretical Study of Combustion and Quenching of Solid Propellant Rocket Motors During Depressurization," Rept. CR 72397, Jan. 15, 1968, NASA; also Hiroki, T., "A Theoretical Study on Combustion and Extinguishment of Solid Propellant Rocket Motors During Rapid Depressurization," Ph.D. thesis, 1967, University of Minnesota.

[9] Hiroki, T., "Combustion in Solid Propellant Rocket Motors Undergoing Depressurization to Produce a Quench," M.S. thesis, 1965, University of Minnesota.

OCTOBER 1969 AIAA JOURNAL VOL. 7, NO. 10

Sensitivity Analysis of Discrete Filtering and Smoothing Algorithms

R. E. GRIFFIN* AND A. P. SAGE†
SMU Institute of Technology, Dallas, Texas

Two problems that occur when filtering or smoothing methods are applied to an actual problem are the choice of the prior statistics and the choice of a mathematical model for the system. The model must be complete enough for an adequate description of the system and also sufficiently simple that the resulting algorithms are computationally feasible. A major tool both in analyzing the effects of these choices and in making the best choice is a sensitivity analysis of the algorithms required in the solution of the filtering and smoothing problems. This investigation presents a sensitivity analysis of the error covariance matrices of the discrete smoothing problem. Algorithms are developed for matrix sensitivity functions for both large and differential errors. Two examples are presented to illustrate the use of the given algorithms: a linearized version for the in-track motion of a satellite traveling in a circular orbit, and a simplified version of an error model of a long-term inertial navigation system which might be used for marine application.

Introduction

DISCRETE versions of time-domain nonstationary filtering and smoothing techniques have proved useful in a wide variety of practical problems. Examples of these problems are estimation of satellite trajectories and optimal utilization of navigational data. Fundamental discussions of both the filtering and smoothing methods appear in Refs. 1 and 2. Difficulties arise from two main sources in practical applications. These sources are the selection of the prior statistics and the choice of a relatively simple mathematical model of the process which is to be filtered or smoothed. A major tool useful in analyzing the effects of these choices is a sensitivity analysis of the algorithms required in the solution of discrete filtering and smoothing methods.

Sensitivity of filtering techniques for large errors has been investigated by Fagin,[3] Nishimura,[4,5] and Heffes[6] for discrete processes. The purpose of this paper is to present what is believed to be the first sensitivity analysis of the discrete smoothing problem as well as a more complete analysis of the discrete filtering problem. Algorithms are presented which allow the computation of matrix sensitivity functions for both large errors and small or differential errors.

Mathematical Models

The process is assumed to be represented by the linear vector difference equation

$$x(k) = \Phi(k,k-1)x(k-1) + G(k-1)w(k-1) \quad (1)$$

where $x(k)$ is a state vector of dimension n, $\Phi(k,k-1)$ is the $n \times n$ state transition matrix, $G(k-1)$ is an $n \times r$ matrix, and $w(k-1)$ is a stochastic input vector of dimension r. Also, linear measurements are assumed to be available in the form

$$z(k) = H(k)x(k) + v(k) \quad (2)$$

where $z(k)$ is a measurement vector of dimension m, $H(k)$ is

Presented as Paper 68-824 at the AIAA Guidance, Control, and Flight Dynamics Conference, Pasadena, Calif., August 12–14, 1968; submitted September 3, 1968; revision received March 10, 1969. This work was partially supported by Air Force Office of Scientific Research, Office of Aerospace Research, U. S. Air Force, under Contract F44620-68-C-0023. R. E. Griffin was supported by a North American Rockwell Fellowship.

* Research Fellow, Information and Control Sciences Center; currently with Texas Instruments Inc., Dallas, Texas.

† Professor and Director, Information and Control Sciences Center. Member AIAA.